Journal of Imaging Science and Technology® 51(5): 438–444, 2007.

High Speed Imaging and Analysis of Jet and Drop Formation

Ian M. Hutchings, Graham D. Martin and Stephen D. Hoath
Inkjet Research Centre, Institute for Manufacturing, Department of Engineering, University of Cambridge, Mill Lane, Cambridge CB2 1RX, United Kingdom
E-mail: gdm31@cam.ac.uk

Abstract. *New techniques have been developed for analyzing, in detail, the shape and development of ink jets and drops. By using flash illumination of very short duration (ca. 20 ns), high quality, single-event digital images of jets and drops can be captured. A computer program, PEJET, has been written to automate the processing of such images and to generate quantitative data about the whole ink stream. From this data, it is then possible to compute the variation in fluid volume, volume flow, and velocity as a function of both position and time. The method has been shown to have high accuracy. The results can be used to study the influences of nozzle design, drive waveform, and fluid properties on jet and drop formation, as well as to provide accurate data for comparison to the results of computational modeling. Examples of results from a drop-on-demand system are presented that illustrate the potential of the method to compare quantitatively the performance of print systems and inks.*
[DOI: 10.2352/J.ImagingSci.Technol.(2007)51:5(438)]

INTRODUCTION

As the range of applications of ink jet systems expands, so the need grows to understand their performance with an ever-widening range of fluids, which are sometimes difficult to print. These may be fluids with complex rheologies or fluids containing high loadings of solid particles.

The visualization of jet and drop formation close to the print head can lead to insights into how the system is behaving.[1–3] From detailed measurement of the shape and size of jets as they develop over time, the volumes and velocities of the jets and the drops which form from them can be computed. These results can then be used to compare the performance of print head designs and printing fluids, and check the validity of numerical models.

This paper describes techniques that have been developed to make such quantitative observations and gives examples of different ways in which this information can be used to explore the performance of inks and print heads.

We have examined model inks jetted from a Xaar drop-on-demand print head as part of development work at the Cambridge Inkjet Research Centre, in some cases replicating previous studies in order to establish techniques and to underpin more novel analyses. In particular, we present some work used to provide input to current theoretical models developed by our research partners.[4]

APPARATUS AND EXPERIMENTAL TECHNIQUES

Figure 1 illustrates the equipment used in this work. The key elements are as follows:

- a high resolution digital camera with a lens system capable of imaging a field of view of a few millimeters, connected to a PC for control and image storage
- an ink jet print head with drive electronics and data source
- a very short duration (~20 ns) flash light source with delivery optics
- means to delay the flash relative to the initiation of the printing event and to measure that delay time accurately

The experiments for the measurements described below used a Xaar 126-200 print head with a linear array of 50 μm diam nozzles. The fluid was a simple semi-transparent UV-curable ink with a Newtonian viscosity of 20 mPa s at 25°C.

Jets and drops emerging from ink jet printers are commonly visualized stroboscopically by creating composite images, superimposing tens or hundreds of individual events in a single frame.[5] This procedure relies on the repeatability of the drop formation process to give the impression of observing individual jets and drops. In some cases, as shown in Figure 2(a), the events are not completely reproducible, which results in some blurring of the image, particularly at long times after drop ejection. For stroboscopic images of this kind the flash duration is typically ≥ 1 μs, which, given the high velocity and small size of the objects being ob-

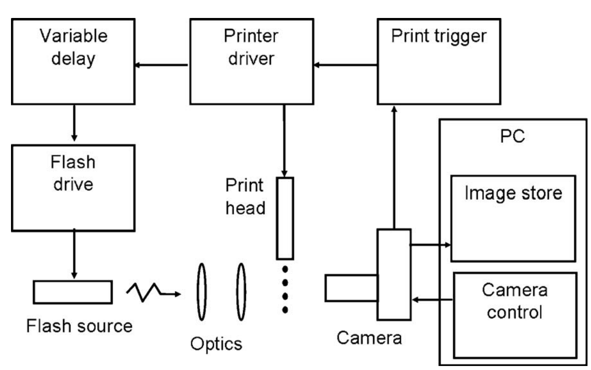

Figure 1. Schematic of apparatus.

Received Mar. 1, 2007; accepted for publication Jun. 20, 2007.
1062-3701/2007/51(5)/438/7/$20.00.

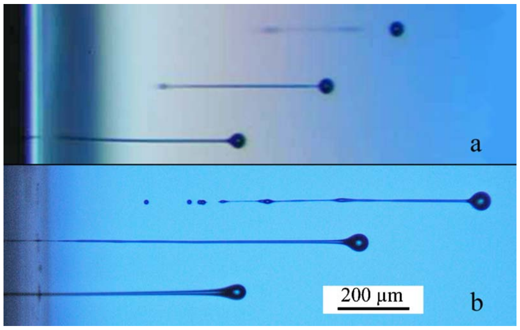

Figure 2. Comparison of images from different techniques: (a) composite image (strobed illumination) and (b) single event (20 ns flash illumination).

served, can result in significant movement blur. However, some information about the development of the jet and drops can be obtained from strobed images by changing the timing or phase of the illuminating flashes relative to the printing event.

Alternatively, a high-speed camera can be used to observe single events as they occur.[6] This requires the use of a camera with a very high framing rate (in megahertz), but typically the pixel resolution of such equipment is poor and only a small number of frames can be captured.

All the images used in this work were obtained by using a short duration (~20 ns) flash and a high resolution still camera. Hence, each captured image was of a unique event. In cases where the events are reproducible, a sequence can be built up by taking pictures of successive events at increasingly greater time intervals from an appropriate event trigger signal. The time delay before firing the flash was set by using signal delay electronics and was measured with an oscilloscope detecting the trigger signal and an output from the flash.

The apparatus shown in Fig. 1 was used to capture individual printing events. A typical image is shown in Fig. 2(b). Because of the very short duration of the flash illumination, there is no significant motion blur. In cases where the events are reproducible, the time development of the event can be investigated by capturing a series of images with different delays. Less reproducible events can also be captured repeatedly and information on their variability determined. Because of the high quality of the imaging, it is possible to determine drop and ligament sizes and shapes and then to use this information to compute drop and ligament volumes. By comparing images within timed sequences, the velocities of the various components of the ink stream can also be determined.

The Xaar XJ126-200 drop-on-demand print head uses a shared-wall piezoelectric design to reduce the head drive voltage needed to form jets of a given velocity. As a result, neighboring nozzles are influenced by the need to actuate the shared walls. The print head can be driven in a single-shot mode that fires a particular group of nozzles at one time, cycling around the three groups A-B-C-A-B-C- and so on, but in our application, a single trigger event caused the print head to print in the sequence A-B-C with fixed short time delays between the three groups. The actual nozzles fired depend on the image presented to the print head. In this work, the images were solid blocks arranged either to print all the nozzles, a designated block of 16 nozzles, a single A-B-C set, or a single nozzle from group A, B, or C, according to the phenomenon under study.

A logic circuit was devised to handle the asynchronous nature of the print command and the print head cycle time clock, in order to ensure reproducible firing of individual nozzles on a timescale of <1 μs. The actual ink jet printing starts at a fixed time in relation to the clock edge, so that without the use of this logic circuit, an additional undesirable timing jitter, equal to the clock cycle time of $\sim$1.75 μs, would be introduced, thereby disrupting pseudosequences obtained with shorter time steps. Residual timing uncertainties were $\sim$0.70 μs, due to randomness in the triggering of some flashes, which were also associated with weaker light output and, thus, darker images. An oscilloscope was used to determine the precise relative timing of the nozzle firing and image capture to a precision of 20 ns. The timings of all images presented here are accurate to <0.1 μs.

IMAGE PROCESSING AND DATA EXTRACTION

To extract quantitative information from the images, it is necessary to analyze them and decide which parts of the image belong to the background and which to the ink drops and ligaments. Standard techniques and various proprietary image processing tools are available to find edges and objects within images.[7] However, there are particular features of these backlit images, which make the use of such tools laborious and sometimes inaccurate. In particular, the background intensity often varies both within each image and from image to image. Within a single image, there is often a thin extended ligament that starts at or near the nozzle. Shading by the nozzle means that the background intensity varies significantly along the length of the ligament. Although the light source provides a very short duration pulse, the nature of the source means that the intensity can vary by 10% or more from image to image. Drops and ligaments from a transparent fluid often show light central regions because light from the bright-field source passes straight through these areas, rather than being refracted away from the optical path as it is at the edges of these features.

The example in Figure 2(b) illustrates some of these issues. An image processing method was developed, which would cope with these variations and artifacts and allow hundreds of images at a time to be analyzed automatically. Physically reasonable assumptions can be made about the objects being imaged to simplify this task. For example, liquid drops and jets will not have holes within them and the edges should be represented by smooth curves at a pixel level. The area within the image in which the drops and ligaments are expected to appear is often known. Fixed features within all the images in a timed sequence can be used to compensate for any small, inadvertent positional movement between the object and the imaging system during the process of image capture.

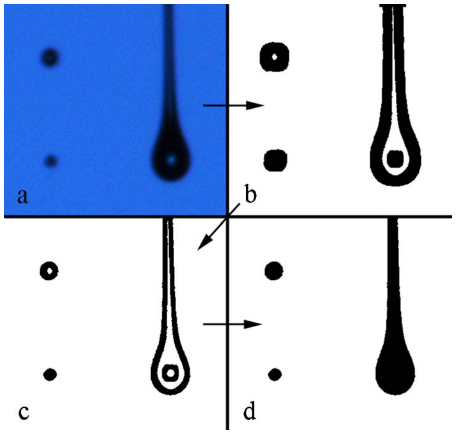

Figure 3. Image processing sequence.

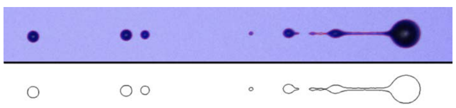

Figure 4. Raw image (above) and processed version (below), showing the results of automated feature selection and edge detection. The largest drop in this image has volume of ~80 pl and the smallest a volume of ~0.2 pl.

The image processing is carried out in several steps, as shown in Figure 3. First, from a selected area of interest (a) a relatively fast but inaccurate technique is used to find the approximate edges of the features by looking for regions of rapid brightness change (b). In the next step (c), the edges are examined in detail to determine which parts of the edges are inside and which parts are outside the feature, based on a threshold level determined by the local ranges of brightness levels. Finally, any "holes" within the features are filled (d).

A computer program, PEJET, was written, which incorporates these processing techniques, together with a way to select a region of interest within a set of images. The program allows a fixed datum to be defined within the image, which is then used to correct for any slight shift of the camera relative to the object over the course of the experiment. The program includes a way to detect and label each feature and to output images indicating the features selected. It also outputs the size data associated with each feature into a text file or spreadsheet. The program can be set up to process a complete set of images (for example, a timed sequence) without operator intervention. Figure 4 is an example of the image output from this program in which the various drops and ligament have been recognized and their edges indicated.

The program has not been optimized for speed because it is not used to process images as they are captured but rather to batch process them subsequently. The sensitivity of the edge detection algorithm can be adjusted to suit the contrast and noise level within the image. It can also be set to reject unwanted or spurious images by defining the region of interest and rejecting spots below a preset level. However, our experience with the images we have captured has been that the program will reliably detect features four or more pixels across. A drop with a diameter of four pixels, with the magnifications typically used, is equivalent to a drop volume of approximately 0.01 pl. The majority of the features observed are traveling at <10 m s^{-1}, and, hence they will move <200 nm during the 20 ns flash duration, which is <0.3 pixels at the typical magnifications used here. We would not expect the feature velocity to have any significant influence on the measurements of volume.

As well as the calculated data the program also outputs images on which the detected edges have been marked. In this way, the proper functioning of the program was ensured by checking the edges detected; in some cases, the volume values were also calculated manually for comparison to those calculated by the program. By flashing a second time after a short delay, two images of exactly the same drop could be captured in the same frame but with the drop moved and with an evolved shape. The program correctly calculates the same volume for these second drop images.

The threshold level selected to make these measurements can have some effect on the measured sizes of the objects. The correct threshold value can be determined in a number of ways. A calibration object of known size can be imaged in the system instead of the jets, and the correct threshold determined by experiment. Alternatively, an image feature of known size (such as the nozzles themselves) can be used to check the accuracy of the measured objects. It is also possible to consider the effect of optical blurring on a sharp edge and to compare edges in the images to those in computed images.

Once the images have been processed, the dimensions and volume of each component of the ink stream can be computed. The camera and print head are usually arranged so that the drop and ligaments travel along the vertical axis of the image. If it is assumed that the ink stream has a circular cross section at all points, then each horizontal line of pixels in an object represents a circular slice through that object. By summing these slices, the volume of the whole stream, or of any horizontal slice through the stream, can be estimated. By comparing such measurements at various stages of drop development, a picture can be built up of how the volume of the object, or any part of it, changes over time. Particular features, such as the tip of the jet or drop or its center of mass, can be tracked, and the method thus provides a powerful tool to generate velocity and flow information.

The evolution of drop and satellite formation can be tracked by dividing the ligament and drop into volume elements and processing successive images to calculate how the volume elements move over time. In the initial image of the sequence, each volume element is chosen to contain a fixed number of pixel slices (Figure 5) and the volume of each element is computed. In subsequent images, the boundaries of each fixed volume element can be determined by summing the volume of ink from each pixel slice until the volume of the element has been reached. In cases where, after a

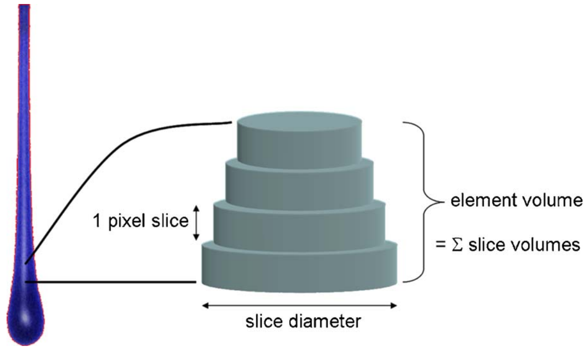

Figure 5. Tracking jet development.

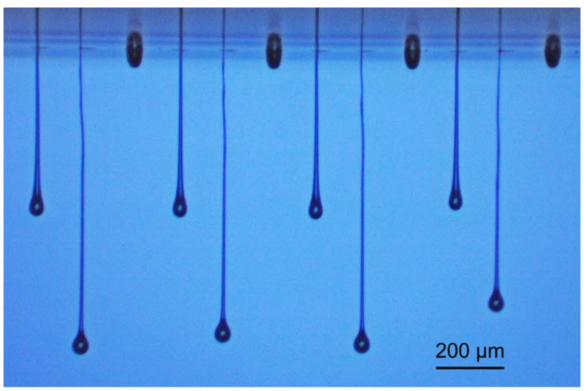

(a)

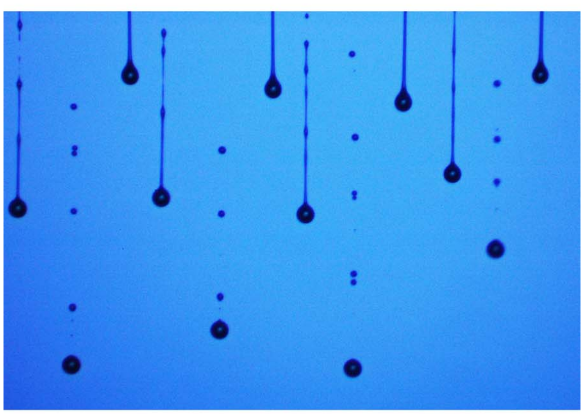

(b)

Figure 6. (a) Group of jets emerging from a Xaar XJ-126 print head. The distance between neighboring nozzles is 137 μm. (b) Image at a later time, for the nozzles shown in (a), showing the evolution of the jets to form ligaments, satellites and main drops.

short initial ink ejection period, the volume of ink external to the nozzle remains substantially constant, the accuracy of this determination can be improved by normalizing the total volumes measured from individual jets in successive images.

RESULTS AND DISCUSSION

In the present work, the print heads were operated with model UV-curable inks and the main ink drops had velocities of ~6 m s^{-1} after 1 mm flight. Ink jets emerging from an array of nozzles (spaced at 137 μm), together with more

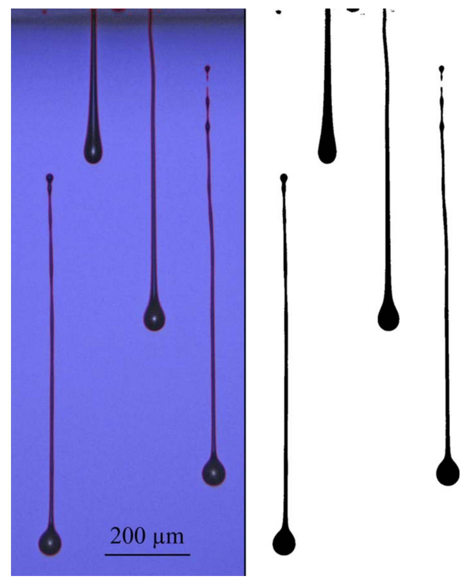

Figure 7. Raw and processed images showing satellite separation and lateral fluctuations.

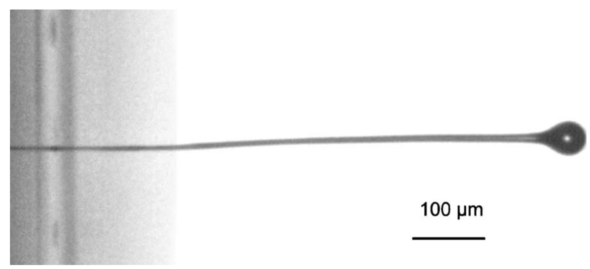

Figure 8. Image showing tail deflection while the ligament is still attached to the nozzle; the orifices of the neighboring nozzles are visible and no other nozzles were fired.

fully developed ligaments, are shown in Figure 6(a). These sharp images resulting from a single ~20 ns flash may be compared to those reported elsewhere (e.g., Ref. 6).

During the early stages of the ejection of ink through the nozzle, the jet ligament becomes rapidly narrower, down to a diameter smaller than that of the orifice at the nozzle plate. This implies that the meniscus must lie within the nozzle, thereby allowing some air to enter the nozzle.

Figure 6(b) displays jets at various later stages, showing ligament stretching, the snapping of ligaments, the formation of satellites, and almost spherical main drops followed by trails of satellites.

Example images are shown in Figures 7 and 8. Figure 7 shows a raw image and corresponding processed image with four jets, one after separation of a tail satellite, with lateral fluctuations, tail ligament thinning, and beading visible. It was possible, in principle, that these tail deflections could occur through the influence of adjacent jets via aerodynamic, acoustic, or other means. Figure 8 was obtained by firing only a single nozzle and demonstrates that deflection of the tail can occur without requiring influences from jets fired from neighboring nozzles. The time after firing at

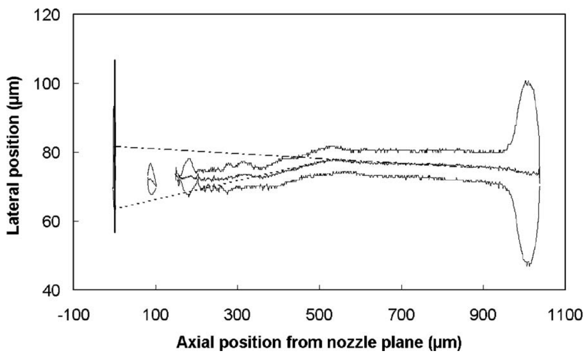

Figure 9. Edge profile for a jet that has broken away from the nozzle (vertical bar), showing a satellite and the center projection (dotted-dashed broken line) of the mass flow from the nozzle. A dotted line represents the lateral deflection of the end of the tail. The lateral scale is exaggerated.

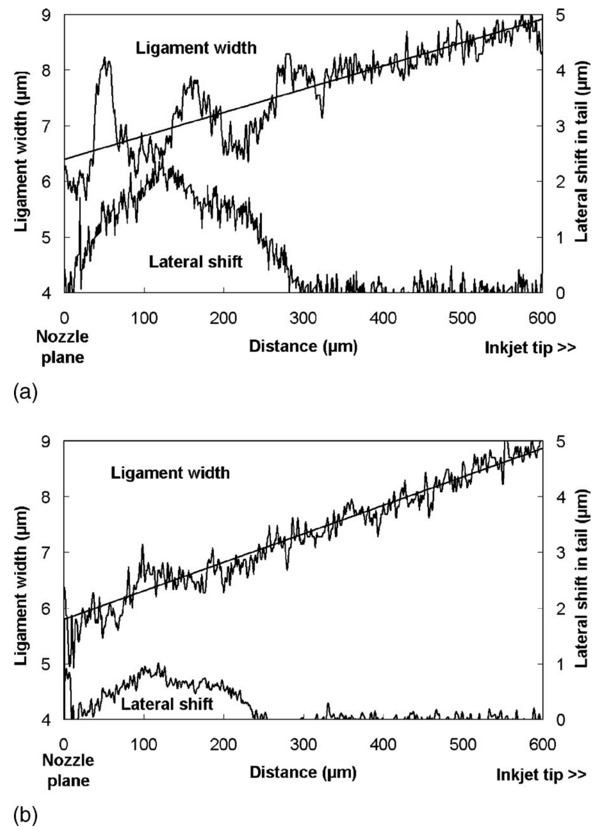

Figure 10. Independence of tail deflection and tail width fluctuations. The center of the jet head was at a position of 888 μm. (b) Tail deflection without width fluctuations at an earlier time for the nozzle of (a). The center of the head was at a distance of 826 μm.

which deflection occurred was similar in all images, whether for single jets or multiple groups, or after cleaning the nozzle plate. Figure 8 also shows the ink patches associated with the orifices of the two unfired neighboring nozzles.

Break off occurs when the stretched ligament thins down and snaps. The two sections then follow independent histories: one will probably move backward into the nozzle orifice and the other will retract toward the main head. Either or both sections may then produce satellites, but usually the initial rupture is close to the nozzle and all satellites originate from the long ligament.

Figure 9 shows the edge profile, derived by the methods described above, from a jet that had broken. The time after the first rupture was enough to allow a satellite to form, and thus, at least one more ligament break had occurred between the nozzle plane and the main ligament. The ligament width fluctuations suggest that other breaks may have been imminent. In this image, the ligament does not appear to point away from the same apparent origin (dotted-dashed line) throughout its length but shows a distinct angular deviation by ~1° at ~520 μm. The later tail section and the satellite appear to point (dotted line) from another location ~10 μm off center. We believe that this implies that the thin ink jet ligament became attached to the edge of the nozzle. It is possible that at some point as it thins, the ligament becomes unstable in a central position and that some small disturbance or asymmetry will then cause it to move to the edge of the nozzle.

Ligament development proceeds, as described earlier, with the stretching of the material between the nozzle plane and the ink jet head. The stretched ligament has a small but finite minimum radius during the process; we have found that the ink jet ligament can be represented by a truncated cone with a specific half angle at the typical distance at which ligament rupture occurs near the nozzle, even if the ligament happens to rupture elsewhere before this, due to the width fluctuations in the thinning ligament.

The tail width fluctuations observed in still-attached ligaments are consistent with net mass movements along a truncated cone shape fitted to the downstream ligament behind the jet head; this cone had a diameter of ~6 μm at the position of the nozzle plane. This is illustrated in Figure 10(a), which shows part of the ~0.9 mm long ligament attached to the nozzle, together with a straight line representing an equivalent undisturbed conical profile matching the ink material volume. The ink jet head is not shown because it was ~50 μm wide. The ligament width is clearly not constant along the length, nor is it zero near the nozzle plane: the minimum ligament width was ~6.4 μm. These data relate to the conditions ~120 μs after printing: strong width fluctuations appear at positions up to ~250 μm from the nozzle. The trajectories of the main drop and its ligament were accurately directed away from the center of the nozzle orifice for a relatively long time, until the tail was apparently disturbed in some way. This suggests that it would be wrong to model the system as axisymmetric. At later times, the ligament tail appeared to be straight but offset, and originating from the edge of the nozzle opening. These effects were not random; they were consistent and different for each nozzle, perhaps reflecting imperfections at the nozzle edges or some other variability, such as nozzle wetting or contamination.

Figure 10(a) also shows the lateral position of a ligament tail plotted on the same scale as the width fluctuations. The center of the ligament lies accurately on the line joining the center of the head to the center of the nozzle back to a distance of 300 μm from the nozzle, then shows a lateral displacement of up to 2 μm before returning to the nozzle

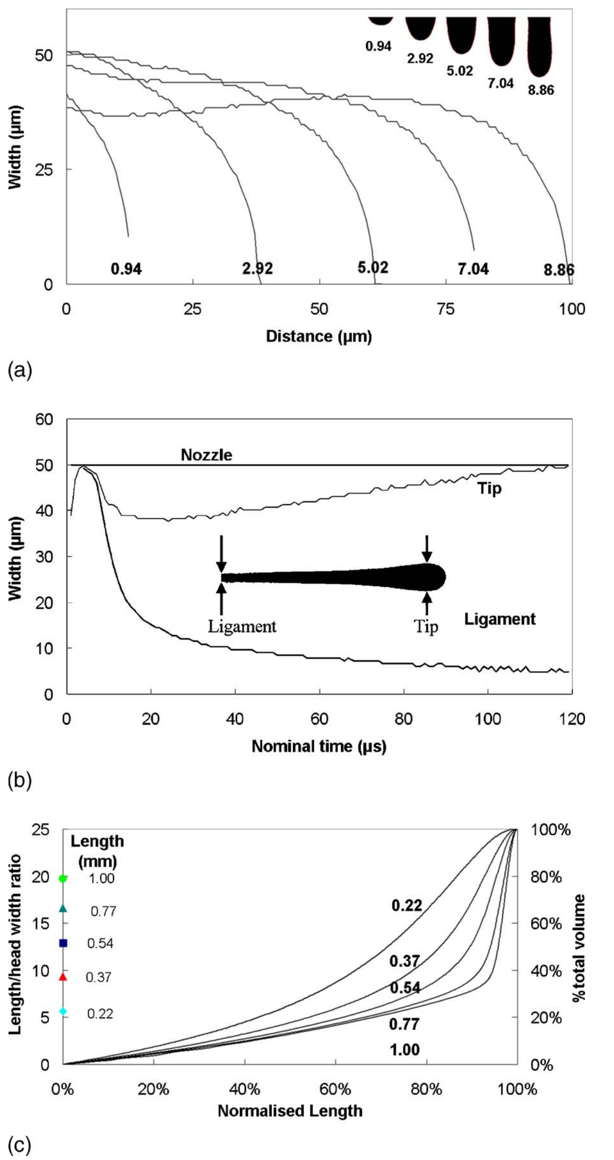

Figure 11. (a) Jet tip profiles for (nominally) 6 m/s ink drops emerging from a 50 μm diameter nozzle, at various times (in microseconds) following emergence. (b) Evolution of the diameters of the jet tip (maximum width) and ligament (minimum width). (c) Percentage of total ink volume along a jet beyond the nozzle plane, for various ligament lengths and ratios of length to main head width.

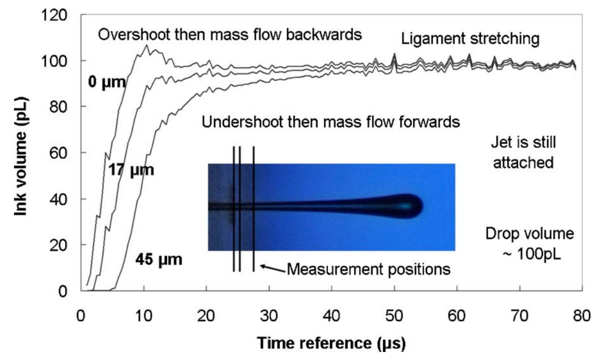

Figure 12. Ink volume passing beyond various downstream planes vs time.

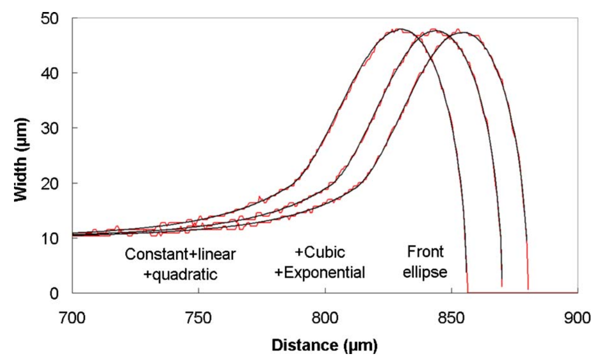

Figure 13. Illustration of the shapes of three long jets that have been fitted by simple empirical functions.

center; the angles between the original ligament axis direction and the tail lay between $-0.5°$ at a distance of 300 μm and $+1°$ at the nozzle plane. Figure 10(b) shows the geometry of a jet from the same nozzle as that in Fig. 10(a), but 16.1 μs earlier. At this earlier time, there are no appreciable width fluctuations but still a significant lateral shift. The phenomena of width fluctuations and lateral shift therefore appear to be independent. Furthermore, the timing and distance information implies that the lateral shift has moved consistently with the axial stretching rate, while width fluctuations have appeared within 20 μs of Fig. 10(b). The graphs in Fig. 10 were generated by averaging the images from three events captured with the same time delay. The small fluctuations derive from the digital nature of the images, which allow only certain values to be obtained for the width and position of the ligament and have an intrinsic error of ± 1 pixel in the width measurement at each point.

Ligament widths and tip diameters vary with time in a systematic fashion. Figure 11(a), for example, shows tip profiles of jets at several short times after emerging from the nozzle. The precision of the technique is illustrated by the linear uncertainty of only 1 pixel ($=0.61$ μm) in this example, similar to the wavelength of the imaging light. Figure 11(b) shows the rapid growth in the tip width of the emerging jet, followed by a rapid fall and then a rise toward the final drop size (corresponding to $\sim$100 pL printed drop volume in this example). The nozzle width is shown for comparison. The minimum ligament width falls quickly after the emergent tip starts necking, and continues to shrink as the ligament stretches.

When the ligament is long and unbroken, the volume lying beyond the nozzle plane stretches as the ligament extends, while the volume fraction in the head increases. For the example shown in Fig. 11(c), the ratio of the length of the ligament to the diameter of the head reaches $\sim$20 before the ligament snaps, at which point there is still $\sim$30% of the total volume in the tail and $\sim$70% in the head section. The total downstream ink volume can be calculated (assuming reproducible ligaments with circular cross section) at different locations. Figure 12 shows that the ink volume beyond the nozzle plane initially overshoots the final drop volume, whereas it undershoots at downstream locations even as

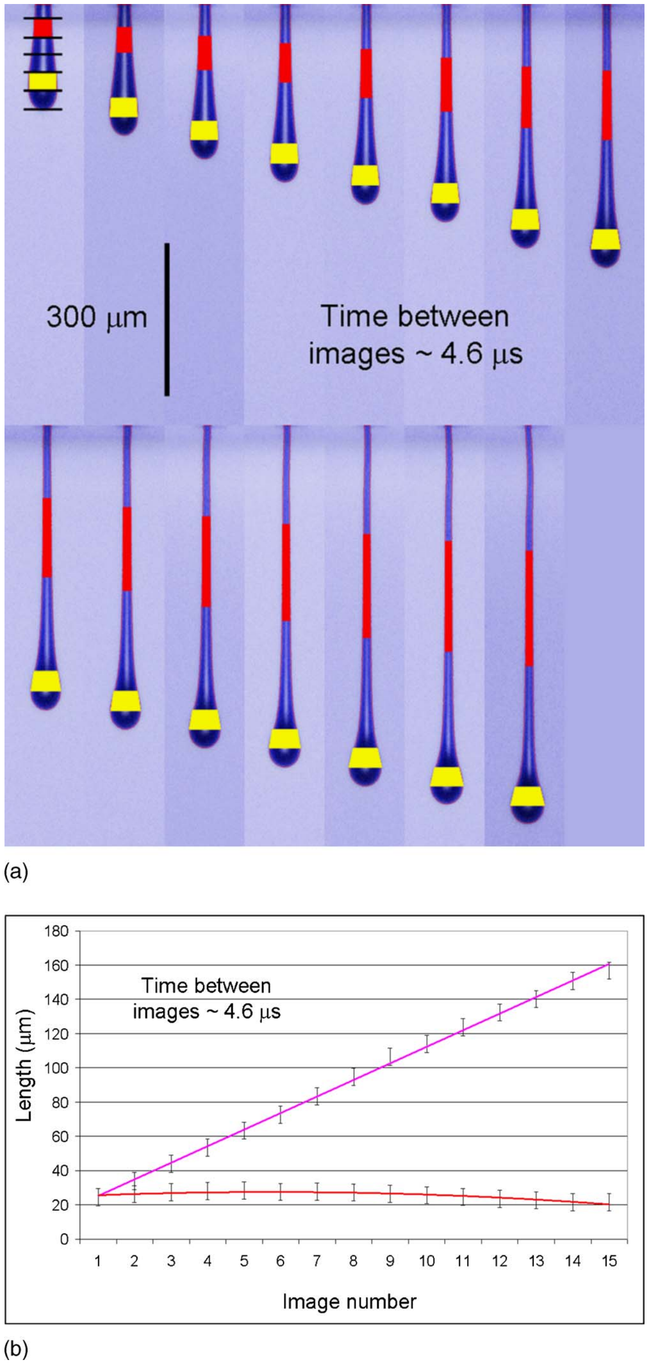

Figure 14. (a) Image sequence and (b) element length evolution.

close as 17 μm (one-third of the nozzle diameter). This indicates that some ink flows backward into the nozzle from very close range, while the rest moves forward as a ligament. In these experiments, the ligament stretched for tens of microseconds before it broke off.

The leading surfaces of the jets studied in this work have been found to be very closely hemispherical, once the emergent phase has passed, as would be expected if the shape is controlled by surface tension and negligible aerodynamic flattening occurs. The rear surface of the head exhibits a shape that can be approximated by constant, linear, and quadratic terms linked to the nozzle plane via ligament stretching, with additional exponential and cubic terms extending to the main drop hemisphere (see Figure 13). As noted above, the ligament behind the main drop tapers smoothly.

Figure 14(a) shows a sequence of images of jets from the same nozzle as they develop over time. Two volume elements have been selected and tracked. The element nearer the nozzle exhibits considerable extension during jet development. In contrast, the element within the head shows a slight contraction, as shown in Fig. 14(b).

CONCLUSIONS

By using flash illumination of very short duration (ca. 20 ns), high quality, single-event digital images of jets and drops can be captured. A computer program, PEJET, has been written to automate the processing of such images and to generate quantitative data about the whole ink stream. From this data, it is then possible to compute the variation in fluid volume, volume flow, and velocity as a function of both position and time. The method has been shown to have high accuracy. The results can be used to study the influence of nozzle design, drive waveform and fluid properties on jet and drop formation, as well as to provide accurate data for comparison to the results of computational modeling.

The level of quantitative information that can be extracted from high speed flash images allows jet profiles and satellite formation to be studied over time. As examples, tail-width fluctuations, lateral deflections, and satellite velocities have been quantitatively analyzed.

It has been shown that, at a late stage, the jet ligament is unstable and tends to move away from the center of the nozzle. At similar times the ligament rapidly forms fluctuations leading to break off and satellites. This late-stage lateral displacement of the ink jet ligament occurs in the absence of aerodynamic, acoustic, or other influences from adjacent jets.

ACKNOWLEDGMENTS

This work was supported by the UK Engineering and Physical Sciences Research Council (EPSRC) and by a consortium of industrial partners within the Cambridge Inkjet Research Centre. Rhys Morgan is thanked for his help in constructing the experimental equipment.

REFERENCES

[1] P. Pierron, S. Allaman, and A. Soucemarianadin, "Dynamics of jetted liquid filaments", *Proc. IS&T's, NIP17* (IS&T, Springfield, VA, 2001) p. 308.

[2] S. Allaman and G. Desie, "Improved ink jet *in situ* visualization strategies", *Proc. IS&T's, NIP20* (IS&T, Springfield, VA, 2004) p. 383.

[3] H. Dong, W. W. Carr, and J. F. Morris, "An experimental study of drop-on-demand drop formation", Phys. Fluids **18**, 072102 (2006).

[4] J. Etienne, E. J. Hinch, and J. Li, "A Lagrangian–Eulerian approach for the numerical simulation of free-surface flow of a viscoelastic material", J. Non-Newtonian Fluid Mech. **136**, 157 (2006).

[5] W. T. Pimbley and H. C. Lee, "Satellite droplet formation in a liquid jet", IBM J. Res. Dev. **21**, 21 (1977).

[6] C. Rembe, J. Patzer, E. P. Hofer, and P. Krehl, "Realcinematographic visualization of droplet ejection in thermal ink jets", *Recent Progress in Ink Jet Technologies II* (IS&T, Springfield, VA, 1999) p. 103.

[7] J. C. Russ, *The Image Processing Handbook*, 4th ed. (CRC Press, Boca Raton, FL, 2002).